Artificial neural network modelling of Nd:YAG laser microdrilling on titanium nitride–alumina composite

R Biswas[1]*, A S Kuar[2], S K Biswas[3], and **S Mitra[2]**
[1]Mechanical Engineering Department, MCKV Institute of Engineering, Howrah, India
[2]Department of Production Engineering, Jadavpur University, Kolkata, India
[3]Central Glass and Ceramic Research Institute, CSIR, Kolkata, India

The manuscript was received on 27 March 2009 and was accepted after revision for publication on 18 August 2009.

DOI: 10.1243/09544054JEM1576

Abstract: Selection of machining parameter combinations for obtaining optimum circularity at entry and exit and hole taper is a challenging task in laser microdrilling owing to the presence of a large number of process variables. There is no perfect combination of parameters that can simultaneously result in higher circularity at entry and exit and lower hole taper. The current paper attempts to develop a strategy for predicting machining parameter settings for the generation of the maximum circularity at entry and exit and minimum hole taper. An artificial neural network (ANN) is used for process modelling of laser microdrilling of titanium nitride–alumina composite and a feed-forward back-propagation network is developed to model the machining process. The model, after proper training, is capable of predicting the response parameters as a function of five different control parameters. Experimental results demonstrate that the machining model is suitable and the optimization strategy satisfies practical requirements. The developed model is found to be unique, powerful, and flexible.

Keywords: artificial neural network modelling, laser microdrilling, circularity, hole taper, optimization

1 INTRODUCTION

Laser beam machining (LBM) has great potential in the modern-day production scenario. LBM is a high-energy-density process that works quickly on complex shapes, is applicable to any type of material, generates no mechanical stress on the workpiece, reduces waste, provides ecologically clean technology, and has the ability to do work in the micro range. The low cost of production has made LBM essential in many industries as well as in household applications. Micromachining is the foundation of the technology to realize miniaturized products. To develop micro-products there must be technological advancement in the field of control, measurement, and assembly. The present research concentrates on control of the factors which affect Nd:YAG laser microdrilling. Several attempts have been made to model the LBM process. Although a good number of fundamental research studies [**1**–**4**] have already been done in the area of laser machining technology, very few have focused on the micromachining area. So, further research is still needed in the area of micromachining for the optimal control of machining parameters.

Kuar *et al.* [**5**] experimentally investigated the influence of computer numeric control (CNC) pulsed Nd:YAG laser microdrilling parameters on the thickness of the heat-affected zone (HAZ) and the phenomenon of tapering of machined microholes on alumina–aluminium interpenetrating composite using response surface methodology. Dhara *et al.* [**6**] developed a feed-forward back-propagation artificial neural network (ANN) to model the laser machining process parameters during the microgrooving operation of die steel and used the developed ANN model to predict and optimize the process performance. Windholz and Molian [**7**] described micromachining of diamond by microsecond pulse Nd:YAG and nanosecond pulse excimer lasers. Ghoreishi

**Corresponding author: Mechanical Engineering Department, MCKV Institute of Engineering, 243 G.T. Road (N), Liluah, Howrah, West Bengal 711204, India.*
email: ranjib_biswas@rediffmail.com

et al. [**8**] employed a statistical model to analyse and compare hole taper and circularity in laser percussion drilling on stainless steel and mild steel. Jackson and O'Neill [**9**] investigated the interaction phenomena of Q-switched, diode pumped Nd:YAG laser using different wavelengths during microdrilling of M2 tool steel by a statistical model. In the area of three-dimensional micromachining, Masuzawa *et al.* [**10**] developed the hole-area modulation method using a semi-transparent mask consisting of a series of small holes, enabling a continuous variable depth just by oscillating the mask in pre-programmed patterns. Kovalenko *et al.* [**11**] reported microdrilling, microcutting and micromilling of semiconductors with green laser. The light of copper-vapour lasers is more strongly absorbed in metals than that of infrared lasers. This leads to deep holes with a small HAZ. Aspect ratios of greater than 40 and surface roughness of the order of 1–2 μm (R_a) were reported by Allen *et al.* [**12**]. Elmes *et al.* [**13**] concluded that laser micromachining is the preferred technique that corresponds with increased speed and automation in biomedical instrumentation such as pin-based picolitre dispensers to take thousands of genetic samples for massive parallel testing. Excimer laser removes only a thin layer of material and has small penetration depth, allowing precise control of the microdrilling depth [**14**]. In several references, the applicability and superiority of the ANN method of analysis have been reported [**15**–**17**].

Titanium nitride–alumina is a ceramic composite containing approximately 40 vol% Al_2O_3 particles dispersed in a TiN matrix. It is a promising material for application as the substrate of the thin-film magnetic recording head in hard disk drive sliders [**18**, **19**], the components of which require high precision in their fabrication. Laser microdilling offers an opportunity for making microholes and other shapes in such thin materials. The material is also finding use in heating elements and other microcomponents for which laser drilling is a convenient machining process. Moreover, as TiN and Al_2O_3 are highly wear- and abrasion-resistant materials [**20**], this ceramic composite has good potential to be used for wear-resistant parts and as a cutting tool material. High chemical stability, low friction coefficient, and high hardness are some of the key properties responsible for its application in components of complex shapes.

Although a large number of research works have been conducted on laser machining, research on the laser microdrilling operation on TiN–Al_2O_3 composite has not been reported so far and thus no technology tables or charts are available in the field of LBM of this composite. Therefore it is imperative to develop a suitable technology guideline for optimum and effective machining of TiN–Al_2O_3 composite. As laser machining is based on the interaction of a laser beam with the workpiece surface, maintaining high hole circularity is a difficult task in laser microdrilling. Also, owing to the focusing characteristics of the laser beam, it is very difficult to produce holes without taper. Nevertheless, from the manufacturing point of view, it is desirable to make the drilled holes circular and without taper. Selection of optimum machining parameter combinations for obtaining higher circularity of the drilled hole at entrance and exit and smaller hole taper is a challenging task in laser microdrilling owing to the presence of a large number of process variables. The current paper attempts to develop a strategy for predicting the optimum machining parameter settings for these geometric features of laser-drilled holes. A feed-forward back-propagation neural network is developed to model the machining processes. The model, after proper training, is used for predicting the response parameters as a function of five different control parameters. These predicted values can be used for optimization purposes.

2 EXPERIMENTAL PLANNING

The experiments were performed on a CNC pulsed Nd:YAG laser machining system manufactured by M/s Sahajanand Laser Technology, India. The detailed specification of the experimental setup is listed in Table 1. The laser beam microdrilling operation was performed on TiN–Al_2O_3 composite specimens having mean thickness of 0.496 mm. The properties of the composite are given in Table 2. In the present research, analysis of the effect of different parameter

Table 1 Specification details of the Nd:YAG laser machining setup

Specification	Description
Laser type	Nd:YAG laser
Wavelength	1064 nm
Mode of operation	Q-switched (pulsed)
Type of Q-switch	Acousto-optic Q-switch
Mode of laser beam	Fundamental mode (TEM_{00})
Mirror reflectivities	Rear mirror 100%, front mirror 80%
Beam diameter $1/e^2$	1 mm
Laser beam spot diameter	100 μm
Pulse width	120 to 150 ns

Table 2 Properties of TiN–Al_2O_3 composite

Property	Units	Value
Density	kg/m^3	4342
Strength (flexural), four-point	MPa	440
Vicker's hardness	GPa	20
Young's modulus	GPa	270
DC resistivity	Ωm	0.25
Thermal conductivity	W/m/K	21 ± 1
Thermal expansion	K^{-1}	8.78×10^{-6}

settings on circularity at entry and exit and hole taper on TiN–Al_2O_3 composite was carried out through ANN modelling.

Based on a literature survey and preliminary investigations, five parameters were chosen as inputs: lamp current, pulse frequency, pulse width, air pressure, and focal length. Selection of the range of process parameter settings was made after performing some pilot experiments using fixed job thickness and type of air pressure. Also, a detailed literature survey was done to select the working range of process parameters. The levels of parameters selected are shown in Table 3.

Table 3 The machining parameters considered and their levels

		Level		
Machining parameter	Units	1	2	3
Lamp current	A	21	22	23
Pulse frequency	kHz	1.2	1.6	2
Pulse width	%	6	9	12
Air pressure	kg/cm^2	1	1.5	2
Focal length	μm	–200	0	200

Experiments were carried out using full factorial combinations of these factors and their different levels. There are other factors that can be expected to have an effect on the measure of performance. In order to minimize their effects, these parameters were held constant: job specimen thickness (0.496 mm) and type of assisted gas (air). An ANN was used to model the process. The validity and accuracy of the developed model has been examined properly. Optimization of multiple responses with the help of predicted responses of the ANN model was done. Five input parameters with three levels could have a total of 3^5 (= 243) combinations of experiments for full factorial design. In total 48 experiments were performed to get the responses. The responses considered were circularity at entry, circularity at exit, and hole taper of the microdrilled holes. Some of the responses (33) were set as target while training of the network was ongoing (Table 4). Out of all the training algorithms, the Levenberg–Marquadt (LM) algorithm is the fastest and consumes the least memory [**16**]; thus the LM algorithm was used for training the network in the present research. The neural network toolbox of MATLAB software was used. After proper training of the network when the desired goal (the

Table 4 Training dataset for the neural network model (the values of variables are normalized)

Sample no.	Lamp current	Pulse frequency	Pulse width	Air pressure	Focal length	Circularity at entry	Circularity at exit	Hole taper (rad)
1	0.913 043	0.6	0.5	0.5	−1	0.9307	0.9102	0.0573
2	1	0.6	0.5	0.5	−1	0.9441	0.8872	0.0584
3	0.913 043	1	0.5	0.5	−1	0.9267	0.9246	0.0558
4	1	1	0.5	0.5	−1	0.9421	0.9045	0.0535
5	0.913 043	1	1	0.5	−1	0.9490	0.9235	0.0467
6	1	1	1	0.5	−1	0.9467	0.9182	0.0493
7	0.913 043	0.6	0.5	1	−1	0.9387	0.9048	0.0677
8	1	0.6	0.5	1	−1	0.9374	0.9180	0.0683
9	0.913 043	0.6	1	1	−1	0.9441	0.9096	0.0667
10	1	0.6	1	1	−1	0.9401	0.9067	0.0640
11	0.913 043	1	1	1	−1	0.9421	0.9214	0.0610
12	1	1	1	1	−1	0.9489	0.9098	0.0704
13	0.913 043	0.6	0.5	0.5	1	0.9140	0.9417	0.0297
14	1	0.6	0.5	0.5	1	0.9402	0.9299	0.0378
15	0.913 043	1	0.5	0.5	1	0.9489	0.9243	0.0357
16	1	0.6	1	0.5	1	0.9480	0.9146	0.0435
17	0.913 043	1	1	0.5	1	0.9131	0.9216	0.0348
18	1	1	1	0.5	1	0.9449	0.9389	0.0366
19	0.913 043	0.6	0.5	1	1	0.9267	0.9093	0.0516
20	1	0.6	0.5	1	1	0.9330	0.9288	0.0594
21	0.913 043	1	0.5	1	1	0.9354	0.9276	0.0399
22	1	0.6	1	1	1	0.9450	0.9392	0.0517
23	0.913 043	1	1	1	1	0.9057	0.9252	0.0495
24	1	1	1	1	1	0.9474	0.9280	0.0561
25	0.956 522	0.8	0.75	0.75	0	0.9344	0.9363	0.0422
26	1	0.8	0.75	0.75	−1	0.9489	0.9192	0.0560
27	0.913 043	1	0.75	0.75	0	0.9401	0.9241	0.0436
28	0.956 522	0.6	1	0.75	0	0.9482	0.9302	0.0463
29	0.913 043	1	1	0.75	0	0.9425	0.9242	0.0444
30	0.956 522	0.6	1	1	0	0.9466	0.9281	0.0546
31	0.956 522	0.8	0.5	1	1	0.9425	0.9390	0.0414
32	0.956 522	0.6	0.5	1	0	0.9381	0.9274	0.0534
33	0.956 522	0.8	0.5	0.5	1	0.9333	0.9359	0.0331

goal set was network output at least 10^{-6} decimal point close to the target value) was achieved, the network was simulated with other input parameter combinations and the network responses compared with the experimental responses (Table 5). Thus validation of the developed model has been checked. The optimum parameter setting for the desired responses was then found by using the responses of the network model.

The thickness of the job sample was measured at different sections using a digital vernier calliper having least count of 0.001 mm. Then microdrilling operations were carried out on the workpiece with the selected parameter settings, keeping the job thickness and type of gas to exert pressure fixed. The diameters of the drilled holes were in micrometre range and the holes were drilled without any relative motion between the laser beam and workpiece. Thus this type of laser drilling belongs to laser percussion drilling. After completion of the experiments, microscopic views of the microdrilled holes at both top (entry) and bottom (exit) surfaces were taken at $10\times$ magnification with the help of an optical measuring microscope (Olympus STM6). The circularity at hole entry and hole exit, and the diameter of the drilled hole at entry and exit, were measured by analysing the microscopic views of holes with image analysis software. The circularity at entry and exit was measured by using the ratio of minimum to maximum Feret's diameters of the hole, which is the distance between two parallel tangents on two opposite sides of the hole (Fig. 1) [**21**]. Microscopic views of microdrilled holes having higher value of circularity at entry and at exit are shown in Figs 2(a) and (b), respectively. After measuring the entrance diameter and exit diameter of the hole, the hole taper was calculated as

$$\text{Hole taper (rad)} = \frac{\text{(hole entrance diameter)} - \text{(hole exit diameter)}}{2\times\text{workpiece thickness}} \quad (1)$$

3 ANN MODELLING OF THE LASER MICROMACHINING PROCESS

ANNs can be used to model complex relationships between inputs and outputs or to find patterns in data. In essence, a neural network can be viewed as a function that maps input vectors to output vectors. The knowledge is presented by the interconnection weight, which is adjusted during the learning stage using the back-propagation learning algorithm that uses a gradient search technique to minimize the mean square error between the actual output pattern of the network and the desired output pattern.

Table 5 Comparison of the developed model with experimental data and the errors in prediction (the values of variables are normalized)

Sample no.	Lamp current	Pulse frequency	Pulse width	Air pressure	Focal length	Experimental circularity at entry	Experimental circularity at exit	Experimental hole taper (rad)	ANN-predicted circularity at entry	ANN-predicted circularity at exit	ANN-predicted hole taper (rad)	% error in prediction of circularity at entry	% error in prediction of circularity at exit	% error in prediction of hole taper
1	0.956 522	0.8	0.5	1	0	0.9409	0.9313	0.0519	0.9395	0.9342	0.0504	0.15	0.31	2.89
2	0.956 522	0.8	0.75	0.5	1	0.9383	0.9351	0.0346	0.8939	0.9396	0.0338	4.73	0.48	3.68
3	1	1	0.75	0.75	−1	0.9455	0.9127	0.0557	0.9489	0.9193	0.0560	0.36	0.72	0.54
4	1	0.8	0.75	0.5	1	0.9463	0.9334	0.0391	0.9037	0.9303	0.0321	4.5	0.33	5.86
5	1	0.8	0.75	0.5	−1	0.9488	0.9196	0.0598	0.9376	0.8993	0.0504	1.18	2.21	2.7
6	0.913 043	1	0.75	0.75	−1	0.9428	0.9218	0.0472	0.9551	0.9232	0.0527	1.3	0.15	2.77
7	0.913 043	0.6	1	0.75	0	0.9447	0.9224	0.0549	0.9387	0.9110	0.0544	0.63	1.23	9.02
8	0.913 043	0.6	1	0.5	−1	0.9494	0.9321	0.0591	0.9631	0.8864	0.0686	1.44	4.9	8.72
9	1	0.6	1	0.5	−1	0.9435	0.9143	0.0645	0.9277	0.8941	0.0631	1.67	2.21	9.74
10	0.913 043	1	0.5	1	−1	0.9320	0.9183	0.0664	0.9381	0.9095	0.0586	0.65	0.96	1.35
11	1	1	0.5	1	−1	0.9346	0.8968	0.0698	0.9183	0.9345	0.0564	1.74	4.2	4.085
12	1	1	0.5	0.5	1	0.9206	0.9301	0.0314	0.9396	0.9328	0.0336	2.06	0.29	8.2
13	0.913 043	0.6	1	0.5	1	0.9030	0.902	0.0528	0.9074	0.9283	0.0389	0.49	2.91	5.71
14	1	1	0.5	1	1	0.9505	0.9415	0.0524	0.9412	0.9489	0.0414	0.98	0.78	5.08
15	0.913 043	0.6	1	1	1	0.9405	0.9306	0.0480	0.9169	0.9095	0.0493	2.51	2.27	2.71
Average % of error												1.63	1.60	4.87
Total average prediction error (%)≈2.70														

Before training the neural network, the architecture of the network has to be decided; i.e. the number of hidden layers and the number of neurons in each layer. As there are five inputs and three outputs, the number of neurons in the input and output layer has to be set to 5 and 3, respectively. According to Fausett [**16**], the back-propagation architecture with one hidden layer is enough for the majority of applications. Hence, only one hidden layer was adopted. A trial-and-error method was employed to optimize the number of neurons in the hidden layer at which the prediction error obtained was a minimum. Prediction error and total average prediction error were defined as

$$\text{Prediction error} = \left|\frac{(\text{experimental result} - \text{predicted result}) \times 100}{\text{experimental result}}\right| \tag{2}$$

and

$$\text{Total average prediction error} = \frac{C_1 + C_2 + H}{3} \tag{3}$$

where C_1, C_2, and H are the average prediction error in circularity at entry, circularity at exit, and hole taper, respectively.

The number of neurons in the hidden layer was changed and the total average prediction error calculated for each case. When the number of neurons in the hidden layer was 11, the total average prediction error was a minimum. The procedure for determining the number of neurons in the hidden layer is shown graphically in Fig. 3. The input parameters

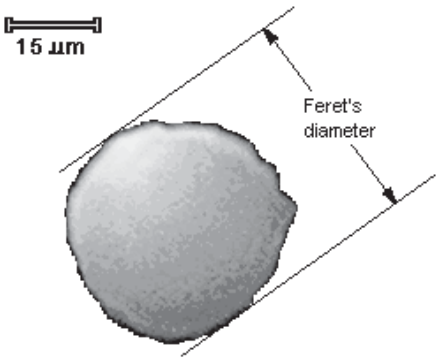

Fig. 1 One of the Feret's diameters

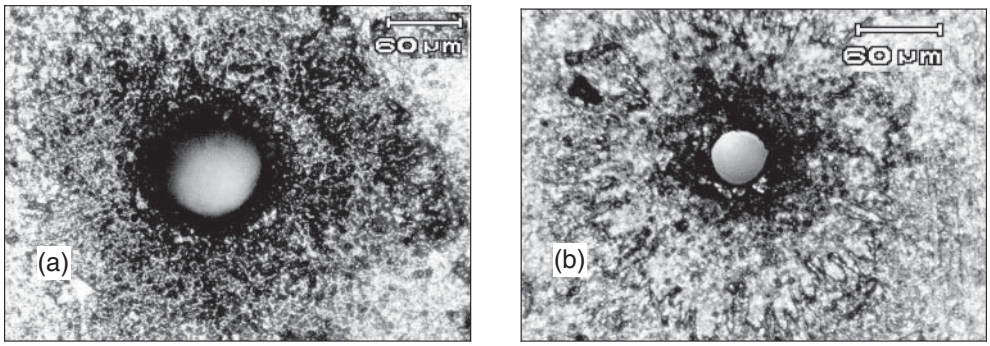

Fig. 2 Microscopic views of microdrilled holes with high hole circularity at entry (a) and exit (b)

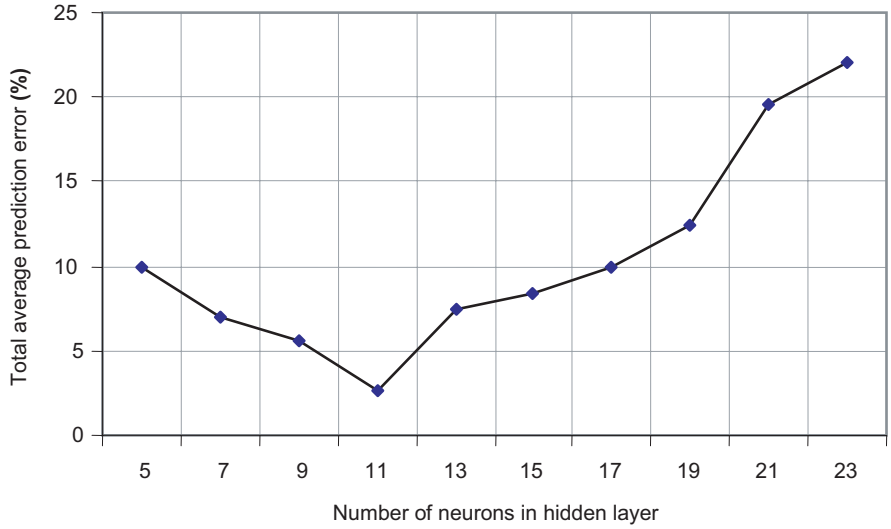

Fig. 3 Plot for determining the number of neurons in the hidden layer

were normalized to lie between –1 and 1. The model developed is a feed-forward back-propagation network having 11 neurons in the hidden layer. So, 5–11–3 is the most suitable network for the task. The developed model is shown schematically in Fig. 4. The experimental results shown in Table 4 were used to train the neural network. The parameters displayed in Table 4 are presented in normalized value. Properly trained back-propagation networks tend to give reasonable answers when presented with inputs that the network has never been fed before. Typically, a new input leads to an output being presented. In back-propagation it is important to be able to calculate the derivatives of any transfer function used.

4 TESTING OF THE DEVELOPED MODEL

An experimental approach was adopted that involved testing the trained neural network against another set of experimental data, illustrated in Table 5, which were drawn randomly from the full factorial dataset. All the input parameters shown in Table 5 are normalized. The errors in prediction are also presented in Table 5. The set of combinations used to predict error is different from those used for training the network. It can be seen from Table 5 that the model-predicted data followed the experimental data very closely: the maximum error in prediction was 4.73 per cent for circularity at entry, 4.90 per cent for circularity at exit, and 9.02 per cent for hole taper. It can be said that the error is within the tolerable limit. Moreover, the average error in the prediction was 1.63 per cent for circularity at entry, 1.60 per cent circularity at exit, and 4.87 per cent for hole taper, which are very small indeed. The total average prediction error of the network (which helps in determining the number of neurons in the hidden layer) was calculated as 2.70 per cent.

5 STRATEGY FOR PARAMETRIC OPTIMIZATION THROUGH THE ANN MODEL

The developed ANN model was used to predict the response parameters, i.e. circularity at entry, circularity at exit, and hole taper, for all combinations of input factors. For better optimization, all input parameters were divided into five levels within their working range as illustrated in Table 6. This helps in generating more predictions ($5^5 = 3125$). Thus more optimal combinations were found as the search was not confined within a small number of predictions. The ANN model was used to predict the circularity at entry, circularity at exit, and hole taper for all possible combinations of factors, i.e. 3125 combinations. Figure 5 shows all of these 3125 responses corresponding to those input parametric combinations. Each point in the plot corresponds to a particular input parameter setting. From all of these predictions (Fig. 5) it was observed that, within the given parametric range, circularity at entry varied between 0.9897 and 0.8281, circularity at exit varied between 0.9887 and 0.8109, and hole taper varied between 0.0210 and 0.0786 rad.

To illustrate the optimization strategy graphically, a few predictions out of the 3125 possible ones are plotted in Figs 6 to 9, so that the philosophy of optimization can be understood more explicitly. The

Table 6 The machining parameters considered divided into five levels

		Level				
Machining parameter	Units	1	2	3	4	5
Lamp current	A	21	21.5	22	22.5	23
Pulse frequency	kHz	1.2	1.4	1.6	1.8	2
Pulse width	%	6	7.5	9	10.5	12
Air pressure	kg/cm^2	1	1.25	1.5	1.75	2
Focal length	μm	−200	−100	0	100	200

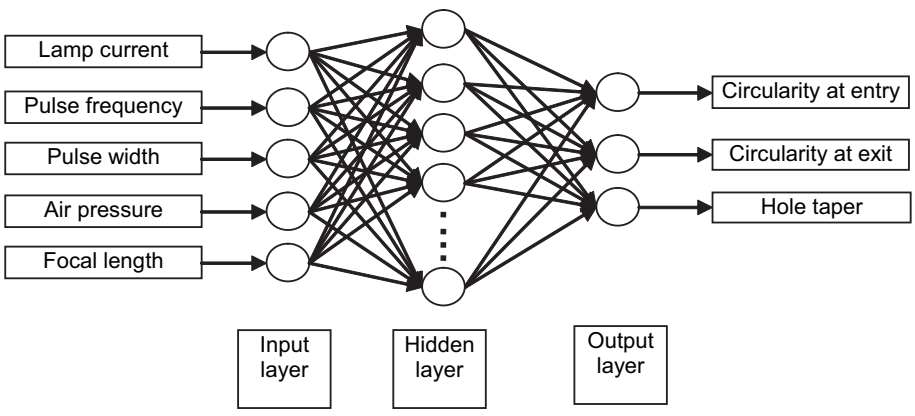

Fig. 4 Configuration of the neural network

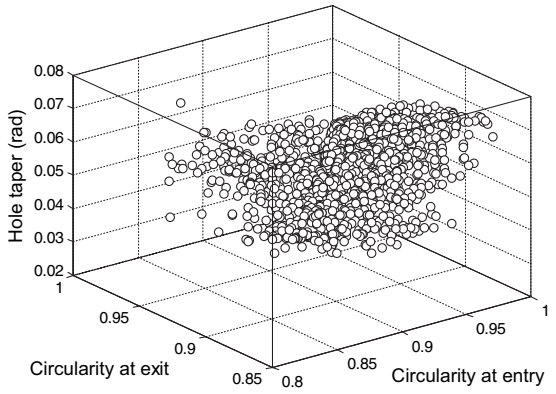

Fig. 5 Prediction of machining characteristics by the ANN model for all 3125 combinations

target is to get the maximum circularity at entry and exit while keeping the hole taper as small as possible. For convenience, in Fig. 6, circularity at entry and circularity at exit are considered as the *x*- and *y*-axis, respectively. In Fig. 7 circularity at entry and inverse of hole taper are considered as the *x*- and *y*-axis, respectively. In Fig. 8 circularity at exit and inverse of hole taper are considered as the *x*- and *y*-axis, respectively. Here the target is to maximize the circularity at entry and circularity at exit in Fig. 6, to maximize the circularity at entry and inverse of hole taper in Fig. 7, and to maximize the circularity at exit and inverse of hole taper in Fig. 8. However, there

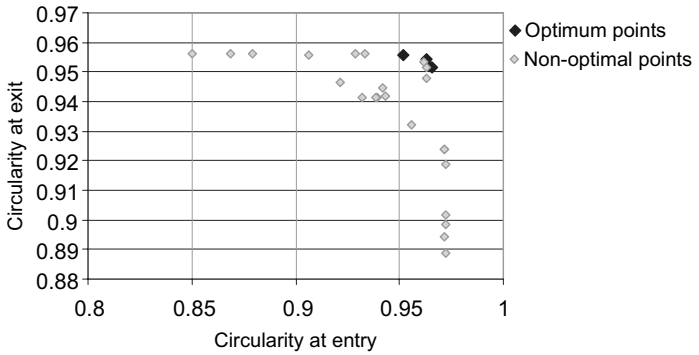

Fig. 6 Search for optimal combinations for circularity at entry and circularity at exit

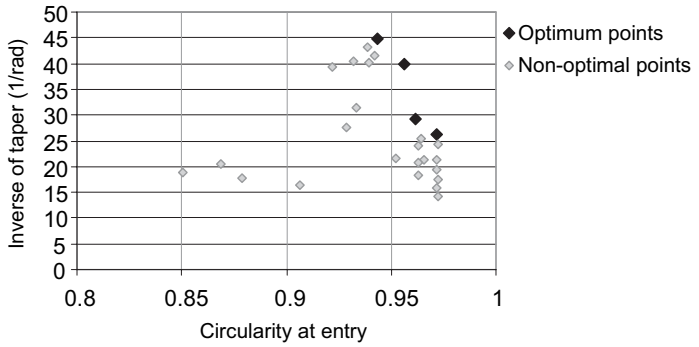

Fig. 7 Search for optimal combinations for circularity at entry and hole taper

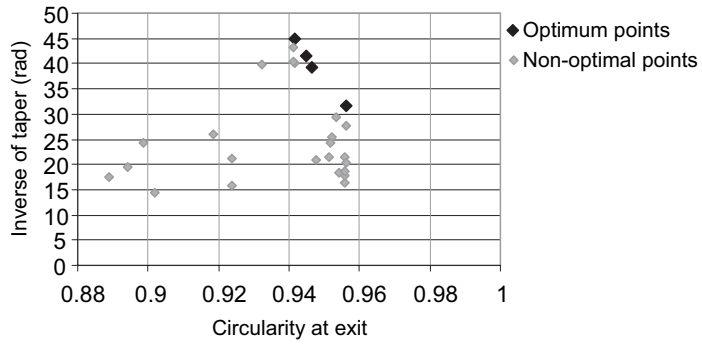

Fig. 8 Search for optimal combinations for circularity at exit and hole taper

cannot be any such single combination that will simultaneously maximize these pairs of responses. Hence there will be several optimal combinations instead of a single optimal combination, and it is truly a multi-objective optimization problem. The optimization search should be for a set of combinations that will give superior output. This set of points corresponds to the optimum points in the plot. Here, superior output means that it is better than any other output at least with respect to one of the process criteria, i.e. circularity at entry or circularity at exit or inverse of hole taper. If one parameter combination yields a better result in both process criteria (Fig. 6, Fig. 7, and Fig. 8), or if it is higher with respect to at least one process criterion and is equal with respect to the other compared with a second parametric combination, then the second combination should never be selected in preference to the first. In other

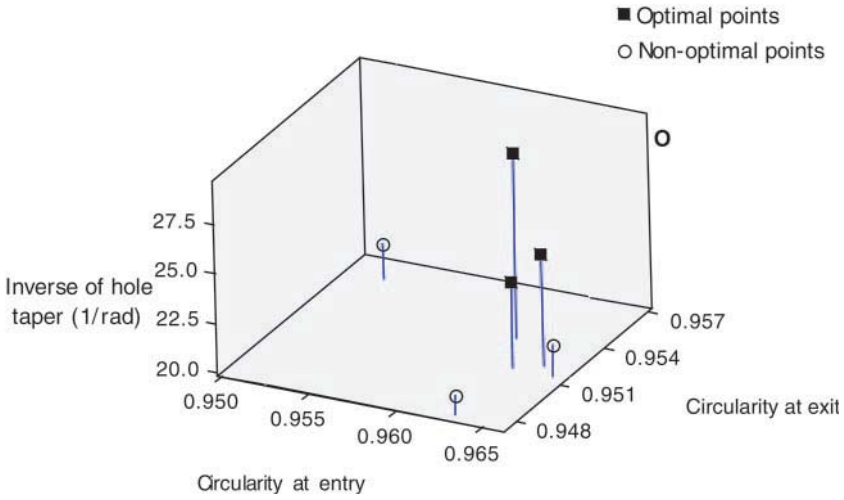

Fig. 9 Search for optimal combinations for the three responses together

Table 7 Technology guideline for optimal machining of TiN–Al_2O_3 composite

	Input parameter					Response		
Sample no.	Lamp current (A)	Pulse frequency (kHz)	Pulse width (%)	Air pressure (kg/cm^2)	Focal length (μm)	Circularity at entry	Circularity at exit	Hole taper (rad)
1	21	2	7.5	1.75	−200	0.9724	0.9017	0.0698
2	21.5	1.6	6	1.25	−200	0.9724	0.8889	0.0568
3	21.5	2	12	1.25	200	0.9721	0.8985	0.0412
4	21	1.8	9	1.25	−100	0.9720	0.9187	0.0383
5	21.5	2	6	1.5	−200	0.9718	0.9237	0.0629
6	21	1.6	9	1.5	−200	0.9718	0.8941	0.0516
7	22	1.6	6	2	−100	0.9717	0.9239	0.0469
8	21.5	2	6	1.75	−100	0.9654	0.9515	0.0467
9	21	2	7.5	1.5	−100	0.9644	0.9520	0.0392
10	22	1.4	12	1.5	0	0.9630	0.9516	0.0414
11	21	1.4	12	1.75	0	0.9630	0.9477	0.0480
12	22	1.2	12	2	−200	0.9628	0.9542	0.0548
13	21.5	1.4	12	1	−100	0.9616	0.9535	0.0342
14	22	2	6	1.25	0	0.9561	0.9323	0.0251
15	21.5	1.2	12	1.25	−200	0.9520	0.9558	0.0463
16	21.5	2	12	1	0	0.9434	0.9418	0.0223
17	21.5	2	12	1	0	0.9422	0.9447	0.0241
18	22.5	1.8	12	1	0	0.9396	0.9415	0.0249
19	22.5	2	10.5	1	0	0.9389	0.9412	0.0232
20	21.5	1.6	9	1	−100	0.9336	0.9563	0.0317
21	22	1.8	10.5	1	0	0.9318	0.9412	0.0248
22	22	2	10.5	1.25	−100	0.9289	0.9562	0.0361
23	21.5	2	9	1.25	0	0.9217	0.9463	0.0255
24	21.5	2	7.5	1.75	−100	0.9063	0.9559	0.0606
25	22.5	1.6	10.5	1.75	0	0.8791	0.9560	0.0566
26	22.5	1.6	12	1.25	100	0.8684	0.9563	0.0490
27	22	2	10.5	1.75	100	0.8504	0.9560	0.0534

Table 8 Final verification experiments and comparison with the optimum results

Sample no.	Lamp current	Pulse frequency	Pulse width	Air pressure	Focal length	Experimental circularity at entry	Experimental circularity at exit	Experimental hole taper (rad)	ANN-predicted circularity at entry	ANN-predicted circularity at exit	ANN-predicted hole taper (rad)	% error in prediction of circularity at entry	% error in prediction of circularity at exit	% error in prediction of hole taper
1	21.5	1.4	12	1	−100	0.9482	0.9443	0.0354	0.9616	0.9535	0.0342	1.41	0.97	3.39
2	22	2	6	1.25	0	0.9426	0.9215	0.0263	0.9561	0.9323	0.0251	1.43	1.17	4.569
3	21.5	1.2	12	1.25	−200	0.9408	0.947	0.0498	0.9520	0.9558	0.0463	1.19	0.93	7.03
4	21.5	2	12	1	0	0.9324	0.9354	0.0238	0.9434	0.9418	0.0223	1.18	0.68	6.30
5	21	1.8	9	1.25	−100	0.9573	0.9005	0.0431	0.972	0.9187	0.0383	1.53	2.02	11.13
6	21.5	2	12	1	0	0.9351	0.9329	0.0246	0.9422	0.9447	0.0241	0.76	1.26	2.03
7	21.5	1.6	9	1	−100	0.921	0.9462	0.0336	0.9336	0.9563	0.0317	1.37	1.07	5.65
8	22	1.2	12	2	−200	0.9534	0.9431	0.0587	0.9628	0.9542	0.0548	0.98	1.17	6.64
9	21	2	7.5	1.5	−100	0.9559	0.9397	0.0442	0.9644	0.952	0.0392	0.89	1.31	11.31
10	21.5	2	6	1.75	−100	0.9503	0.9416	0.0492	0.9654	0.9515	0.0467	1.59	1.05	5.08
Average % of error												1.23	1.16	6.31
Total average prediction error (%)≈2.90														

words, graphically, a point is not optimal if there is any other point that is above and right to the first point. If both the points have the same coordinates, both will be considered. Now it is quite clear why some points situated at the boundary were referred to as optimum points in Figs 6 to 8. The multi-objective optimization result for all three responses together is shown in Fig. 9, in which circularity at entry, circularity at exit, and inverse of hole taper are considered along three axes. Here the target is to maximize circularity at entry and exit and inverse of hole taper together. So it can be concluded from the surface plot that the points nearer to point O (which indicates maximum circularity at entry and at exit (1) and minimum value of hole taper) gives superior output for all three responses together. The parameter settings for which better results can be obtained are shown in Table 7 along with the predicted responses. To further verify the proposed model, another set of experiments was carried out and compared with the predicted results. For this purpose optimum parameter settings were been selected and compared, with the results also shown in Table 7. It was observed that the predicted value was quite close to the experimental result. The experimental result and the predicted optimum result along with the corresponding prediction error are shown in Table 8.

6 CONCLUSIONS

In the present research, Nd:YAG laser beam microdrilling of TiN–Al_2O_3 composite has been carried out and an advanced optimization strategy has been used to determine the optimal combination of control parameters. The method used was capable of optimizing the important geometric features of the hole, such as circularity at entry, circularity at exit, and hole taper, within specified limits. A feed-forward back-propagation neural network was used to construct the laser beam process model. It has been found that among several neural configurations, a feed-forward back-propagation ANN of type 5–11–3, having one hidden layer with 11 neurons, can provide the best prediction. Validation experiments for the developed model were conducted and the prediction accuracy of the model was found to be quite good. A graphical method was used to search for the optimal combinations of parameters from the set of all possible combinations of parameter settings, i.e. 3125 predictions. Twenty-seven parametric combinations were identified out of these 3125 combinations, which will act as a technology guideline for effective machining of the material. Through the optimization strategy, one can obtain optimal parametric combinations that will lead to efficient utilization of laser beam microdrilling in practice. This approach

has high potential to be used in other machining processes.

REFERENCES

1 **Meijer, J.** Laser beam machining (LBM), state of the art and new opportunities. *J. Mater. Process. Technol.*, 2004, **149**, 2–17.

2 **Chen, T. C.** and **Darling, R. B.** Parametric studies on pulsed near ultraviolet frequency tripled Nd:YAG laser micromachining of sapphire and silicon. *J. Mater. Process. Technol.*, 2005, **169**, 214–218.

3 **Li, Q., Zheng, Y., Wang, Z.,** and **Zuo, T.** A novel high-peak power double AO Q-switched pulse Nd:YAG laser for drilling. *Optic Laser Technol.*, 2005, **37**, 357–362.

4 **Sun, Z., Li, R., Bi, Y., Hu, C., Kong, Y., Wang, G., Zhang, H.,** and **Xu, Z.** Experimental study of high-power pulse side-pumped Nd:YAG laser. *Optic Laser Technol.*, 2005, **37**, 163–166.

5 **Kuar, A. S., Paul, G.,** and **Mitra, S.** Nd:YAG laser micromachining of alumina–aluminium interpenetrating phase composite using response surface methodology. *Int. J. Machining Machinability Mater.*, 2006, **4**, 432–444.

6 **Dhara, S. K., Kuar, A. S.,** and **Mitra, S.** An artificial neural network approach on parametric optimization of laser micro-machining of die-steel. *Int. J. Adv. Mfg Technol.*, 2008, **39**, 39–46.

7 **Windholz, R.** and **Molian, P.** Nanosecond pulsed excimer laser machining of CVD diamond and HOPG graphite. *J. Mater. Sci.*, 1997, **32**, 4295–4301.

8 **Ghoreishi, M., Low, D. K. Y.,** and **Li, L.** Comparative statistical analysis of hole taper and circularity in laser percussion drilling. *Int. J. Machine Tools Mfg*, 2002, **42**, 985–995.

9 **Jackson, M. J.** and **O'Neill, W.** Laser micro-drilling of tool steel using Nd:YAG lasers. *J. Mater. Process. Technol.*, 2003, **142**, 517–525.

10 **Masuzawa, T., Olde Bennker, J.,** and **Eindhoven, J. J. C.** A new method for three dimensional excimer laser micromachining by hole area modulation (HAM). *CIRP Ann.*, 2002, **49**, 139–142.

11 **Kovalenko, V., Anyakin, M.,** and **Uno, Y.** Modelling and optimisation of laser semiconductor cutting. In Proceedings of the ICALEO Laser Microfabrication Conference, 2–5 October 2001, vol. 90, pp. D82–D92 (LIA, Orlando, Florida).

12 **Allen, D., Almond, H.,** and **Logan, P.** A technical comparison of micro-electro-discharge machining, micro drilling and copper vapour laser machining for the fabrication of ink jet nozzles. *Proc. SPIE*, 2000, **4019**, 531–540.

13 **Elmes, S., Pearson, J., Moore, D. F., Rutterford, G. A., Bell, A. I., Rivera, N.,** and **Knowles, M. R. H.** Laser machining of micro reservoir pins for gene analysis and high throughput screening. In Proceedings of the ICALEO Laser Microfabrication Conference, 15 October 2001, Paper M303 (LIA, Orlando, Florida).

14 **Ready, J. F.** *LIA handbook of laser materials processing*, 2001 (Magnolia, Orlando, Florida).

15 **Sarkar, S., Mitra, S.,** and **Bhattacharyya, B.** Parametric optimisation of wire electrical discharge machining of γ-titanium aluminide alloy through an artificial neural network model. *Int. J. Adv. Mfg Technol.*, 2006, **27**, 501–508.

16 **Fausett, L.** *Fundamentals of neural networks: architectures, algorithms and applications*, 1994 (Prentice-Hall, New York).

17 **Haykin, S.** *Neural networks: a comprehensive foundation*, 2002 (Pearson Publication, Harlow, UK).

18 **Jiang, M., Hao, S.,** and **Komanduri, R.** On the advanced lapping process in the precision finishing of thin-film magnetic recording heads for rigid disc drives. *Appl. Phys.*, 2003, **A77**, 923–932.

19 **Liu, F. X., Yao, K. L.,** and **Liu, Z. L.** Different substrate materials effect on structure of ta-C films by Raman spectroscopy for magnetic recording sliders. *J. Non-Cryst. Solids*, 2007, **353**, 2545–2549.

20 **Casas, B., Wiklund, U., Hogmark, S.,** and **Llanes, L.** Adhesion and abrasive wear resistance of TiN deposited on electrical discharge machined WC–Co cemented carbides. *Wear*, 2008, **265**, 490–496.

21 **Allen, T.** *Particle size measurements*, edition 3, 1981 (Chapman and Hall, London, UK).